Journal of Colloid and Interface Science **244,** 230–238 (2001)
doi:10.1006/jcis.2001.7971, available online at http://www.idealibrary.com on IDEAL®

An Analysis of Zinc Sorption to Amorphous versus Crystalline Iron Oxides Using XAS

Paras Trivedi,* Lisa Axe,*,[1] and Trevor A. Tyson†

*Department of Civil and Environmental Engineering, New Jersey Institute of Technology, Newark, New Jersey 07102; and †Department of Physics, New Jersey Institute of Technology, Newark, New Jersey 07102

Received May 17, 2001; accepted September 14, 2001

This research probes the mechanisms of Zn adsorption on hydrated oxides of iron (HFO and goethite) using XAS. A systematic investigation reveals that Zn^{2+} upon sorption to HFO retains its hydration shell ($N \sim 6$ oxygens, $R \sim 2.18$ Å), irrespective of pH and adsorbate loading. Furthermore, the absence of second-shell contributions in combination with the temperature dependence of the structural parameters confirms outer-sphere adsorption complexes with HFO. In a coprecipitation study, the local coordination environment was consistent with Zn adsorption to HFO. On the other hand, Zn^{2+} strongly adsorbs to goethite forming a tetragonal structure ($N \sim 4$ oxygens and $R \sim 1.97$ Å). Evidence of two Fe^{3+} ions in the second shell at approximately 3.51 Å suggests an inner-sphere adsorption complex with goethite. Results demonstrate that even though the local structures of HFO and goethite are similar, the surface sites available to transition metals like zinc are vastly different. Overall, these spectroscopic analyses are consistent with macroscopic observations.

Key Words: **iron oxides; zinc; adsorption; coprecipitation; XAS.**

INTRODUCTION

The fate of heavy metals like zinc in aquatic environments is largely governed by sorption to oxides of iron (1, 2). These oxides exist in many forms ranging from the amorphous and metastable ferrihydrite to crystalline ones such as goethite and hematite (3). Manceau and co-workers have shown that even though goethite and hydrous ferric oxide (HFO) have similar structures, the lengths of their octahedral chains and hence their site densities differ (4–6). A comparison of the macroscopic results shows that amorphous oxides such as ferrihydrite (also known as HFO) have large sorption capacities for metal contaminants as compared to crystalline oxides such as goethite (8–13). On the other hand, thermodynamic analyses suggest that while transition metals like Zn may be chemically sorbed to goethite (13, 14), adsorption to HFO involves physical forces (9, 10, 13). Long-term studies reveal that intraparticle diffusion is the rate-limiting mechanism for sorption to the microporous oxides, and thus zinc sorption may require from a few months to a few years to reach equilibrium (10, 15–17). Similar studies with goethite indicate microporosity is not significant (13). Macroscopic experiments provide information on bulk equilibrium and kinetic processes; however, to determine the molecular mechanisms, X-ray absorption spectroscopy (XAS) is needed.

XAS has proven to be a powerful tool in environmental research as it selectively probes the local coordination environment of a species over a wide range of concentrations. This structural information, including the identification of neighbors, their coordination numbers, and bond distances, provides contaminant sorption mechanisms under environmentally relevant conditions. Extensive studies have been conducted in the past to establish the adsorption mechanisms for different metal ions with various hydrated iron oxides. A large number of these studies have shown that metal ions sorb to these oxides through inner-sphere complexes: Cr(III) to goethite and ferrihydrite (18); Cd to a "two-line ferrihydrite" type of hydrous ferric oxide and to goethite (6); selenate to two-line ferrihydrite and goethite (5); U(VI) to ferrihydrite (19); As(V) and Cr(VI) to goethite (20); Zn to goethite (21); Pb to goethite (22–24) and to hematite (22); Hg(II) to goethite (25); and Cu and Pb to two-line ferrihydrite (17). In contrast, other studies of iron oxide systems report outer-sphere types of adsorption mechanisms, where the adsorbate ions retain their waters of hydration; these include ZnEDTA sorption to goethite (21), Sr sorption to HFO (26), PbEDTA sorption to goethite (27), and Sr sorption to goethite (28).

Limited research has been conducted in coordinating macroscopic and spectroscopic observations for Zn sorption to metal oxides and clay minerals. Earlier work on zinc sorption to ferrihydrite (29) and zinc–ferric hydroxide coprecipitation (1) reported the transition from a six-fold coordination of zinc ions in the aqueous phase to a four-fold one sorbed to the surface. On the other hand, Schlegel *et al.* (21) observed that zinc ions in a nitrate-based electrolyte as well as in a complex with EDTA retained the octahedral hydration shell upon sorption to goethite. Recently Trainor *et al.* (30) studied Zn^{2+} sorption to α-alumina powders as a function of sorption density and pH; they found Zn ions in tetrahedral coordination at low sorption densities. At higher sorption densities, although they observed six highly disordered oxygen atoms in the first shell

[1] To whom correspondence should be addressed. Fax: (973) 596–5790. E-mail: axe@adm.njit.edu.

0021-9797/01 $35.00

at approximately 2.02 Å, they surmised that two of the six were from the alumina surface. Furthermore, on the basis of their analyses they concluded that at low sorption concentrations, Zn ions formed predominantly an inner-sphere bidentate complex with AlO_6 polyhedra, whereas at higher sorption densities Zn formed a mixed-metal hydroxide coprecipitate with aluminum (30). Likewise, XAFS studies of Zn sorption to pyrophyllite as a function of surface loading (0.1–1.6 μmol m^{-2} of pyrophyllite) and time revealed the formation of a Zn–Al layered double hydroxide where the crystalline stability increased with aging (31). To complement the macroscopic studies of Zn sorption to HFO and goethite presented in the accompanying paper (13), a systematic analysis at the molecular level was conducted as a function of pH, adsorbate loading, and method of contact (adsorption versus coprecipitation).

In this research, the primary objective was to identify and compare Zn sorption mechanisms to HFO and goethite adsorbents as a function of pH, adsorbate loading, and method of contact on the basis of macroscopic studies (10, 11, 13). Overall, this research aides in distinguishing different types of adsorption complexes such as inner- and outer-sphere ones, which are crucial in understanding contaminant mobility and bioavailability in subsurface systems.

EXPERIMENTAL METHODS AND ANALYSES

Sample Preparation

HFO was prepared following the method described by Dzombak and Morel (32). The characteristics and properties of this HFO have been discussed previously (8, 13, 33). Adsorption samples were prepared at pH 7 and 25°C for the following sorption densities: 1×10^{-3} and 1×10^{-2} mol of Zn g^{-1} of HFO. To understand the sorption mechanism as a function of pH, samples with an adsorbate loading of 1×10^{-3} mol of Zn g^{-1} of HFO were studied at pH 6 and 8. Finally, the local structure of Zn^{2+} was also examined in a Zn–HFO coprecipitate sample prepared at pH 7 and 25°C; the Zn concentration in this sample was 1×10^{-3} mol of Zn g^{-1} of HFO. The purpose of this study was to examine whether a coprecipitate formed or the Zn ion adsorbed to the oxide surfaces prior to aggregation during precipitation.

Goethite was synthesized by employing the modified Atkinson's method and this synthesis process along with the goethite characterization are detailed in the accompanying paper as well as elsewhere (11, 13). Zinc adsorption to goethite was studied as a function of pH and loading with one sample of 1.2×10^{-5} mol of Zn g^{-1} of goethite at pH 6 and another with 2.0×10^{-5} mol of Zn g^{-1} of goethite at pH 7. These sorption densities approximately represent the adsorption capacity of goethite for transition metals like Zn (11, 13).

The sorbed Zn concentration was determined using ^{65}Zn as a tracer in duplicate samples (10), where the activity was measured with a Beckman LS6000SE liquid scintillation counter. Except where otherwise stated, adsorption samples were equilibrated for 4 h under turbulent hydraulic conditions (Reynolds number $[Re] \geq 3.0 \times 10^5$ with respect to the reactor length) before the solid phase was separated from the supernatant by centrifuging at 8000 rpm (rotor radius of 7.76 cm) for 20 min. These wet pastes were loaded into aluminum or acrylic sample holders, which were sealed with Mylar windows to prevent the loss of moisture. Reference compounds, with well-known structures, chosen for XAFS analyses included zinc carbonate hydrate ($ZnCO_3 \cdot nH_2O$), zincite or zinc oxide (ZnO), zinc oxide hydrate ($ZnO_3 \cdot nH_2O$), zinc ferrite ($ZnFe_2O_4$), and a 1×10^{-3} M $Zn(NO_3)_2$ solution at pH 1.

XAS Data Collection

XAS data were acquired on beamline X-11A at the National Synchrotron Light Source (NSLS), Brookhaven National Laboratory, where the electron beam energies were 2.528 and 2.8 GeV with an average beam current of 180 mA. All Zn spectra were collected over the energy range of 9509–10,408 eV. The samples of Zn sorbed to HFO were measured in fluorescence mode placed at 45° to the incident beam using a Lytle detector filled with Ar gas. To minimize the background, a 6-μm Cu filter (Z-1 filter) with one aluminum foil was placed between the sample and the soller slits, which was used to block most of the filter refluorescence. Harmonic rejection was achieved by detuning the monochromator 20% of I_o. For Zn–goethite adsorption samples, XAS spectra were collected in fluorescence mode using a multielement Ge solid-state detector. For these samples, the monochromator was detuned to 70% of the fully tuned I_o to operate the detector in the linear regime. Prior to analyses, Zn spectra from each of the multielement detector elements were inspected individually, and then added up to obtain the total fluorescence data. The XAS data of the reference compounds were collected in transmission mode at room temperature (298 K) and 77 K. The associated absorption lengths at the Zn K-edge were found to be 8 μm for ZnO, 19 μm for $ZnO \cdot nH_2O$, 16 μm for $ZnCO_3 \cdot nH_2O$, 17 μm for $ZnFe_2O_4$, and 2 mm for 1×10^{-3} M $Zn(NO_3)_2$.

XAS Data Analyses

The XAS spectra were analyzed using WinXAS 97 (Version 1.0) (34). For each scan, the background X-ray absorbance was subtracted by fitting a linear polynomial through the pre-edge region. The edge jump of a background-corrected spectrum was normalized with a linear polynomial over 9.759–9.959 keV. The threshold energy (E_o) was determined from the first inflection point in the edge region and was used to convert the spectra from energy to k-space. A spline function was employed to account for the atomic absorption in the absence of backscattering contributions over the range 2.3–14.0 $Å^{-1}$. This isolated function produced the XAFS function ($\chi(k)$), which was then weighted by k^3 to enhance the higher k-space data. A Bessel window function was used in Fourier transforms to produce the radial structural function (RSF) over 2.65–13.65 $Å^{-1}$ for all Zn standards except the $Zn(NO_3)_2$ solution, which was filtered over 2.3–9.2 $Å^{-1}$. All

adsorption samples were Fourier transformed over 2.3–9.2 $Å^{-1}$ as well. These RSFs are not corrected for phase shifts.

To obtain the structural information, the Fourier transforms were fit with a reference model generated using FEFF7 (35), where all the parameters except the amplitude reduction factor (S_0^2) were allowed to float. A comparison of the $Zn(NO_3)_2$ solution spectra collected in transmission mode with that of the fluorescence revealed an averaged S_0^2 of 0.70; this S_0^2 was employed in the fitting process for the adsorption samples. In the case of fitting multiple shells, the E_o shift was constrained to be equivalent for all shells. All samples and standards except $ZnCO_3 \cdot nH_2O$ were fit with chalcophanite ($ZnMn_3O_7 \cdot 3H_2O$), where to obtain Zn–Fe contributions, the chalcophanite structure was modified by replacing Mn with Fe (36, 37). Typically, a chalcophanite crystal consists of edge-sharing $Mn(IV)O_6$ octahedra that alternate with layers of Zn ions and water molecules (36, 38). For $ZnCO_3 \cdot nH_2O$, hydrozincite ($Zn_5(OH)_6(CO_3)_2$ was used for fitting (39).

RESULTS AND DISCUSSION

Zn Standards

The XAS spectra of Zn standards in Fig. 1 show that for each standard the χ-amplitude decreased with increase in temperature as a result of the increase in contributions from thermal vibrations. Unlike other Zn standards, the spectra of aqueous zinc nitrate show only first-shell contributions as would be expected. Figure 1 also includes chalcophanite, which was generated theoretically using FEFF7. Resultant Fourier transforms along with the fits for these standards are presented in Fig. 2 and in Table 1 where their structural parameters generated from the fits are compared with those of their known structure (shown in parentheses). For aqueous zinc nitrate the first shell consisted of 5.83 ± 0.39 O atoms at an average radial distance (R) of 2.18 ± 0.04 Å; these parameters are indicative of the octahedral coordination of Zn by O in the aqueous solution. Recently, Trainor *et al.* (30) reported 6.1 O atoms at 2.07 Å around Zn from XAFS studies with a 10 mM $Zn(NO_3)_2$ at pH 3.6; Numako and Nakai (40) estimated the Zn–O distance in 0.1 M $Zn(NO_3)_2$ to be approximately 2.09 Å when they assumed six oxygen atoms surrounded Zn in the primary hydration shell. From XAFS studies with an aqueous ZnEDTA solution at pH 3, Schlegel *et al.* (21) found two sets of O atoms contributing to the first shell: 3.5 atoms at 2.01 Å and 3.2 atoms at 2.19 Å. For ZnO and for $ZnO \cdot nH_2O$, the first shell was tetragonal comprising 3.3–4 O atoms ($R = 1.96$ Å) and the second shell of 11.7–14.3 Zn atoms ($R = 3.21$–3.22 Å) was also observed; these results are consistent with those reported by Trainor *et al.* (30). Pandya *et al.* (41) investigated the local structure of Zn^{2+} in concentrated aqueous hydroxide solutions. Using single and multiple scattering, they determined that the Zn ions are in a tetrahedral configuration with a Zn–O bond distance of 1.96 Å; however, no satisfactory fits were obtained for the second shell. In the present research, the XAS spectra of $ZnCO_3 \cdot nH_2O$ were fitted with hydrozincite,

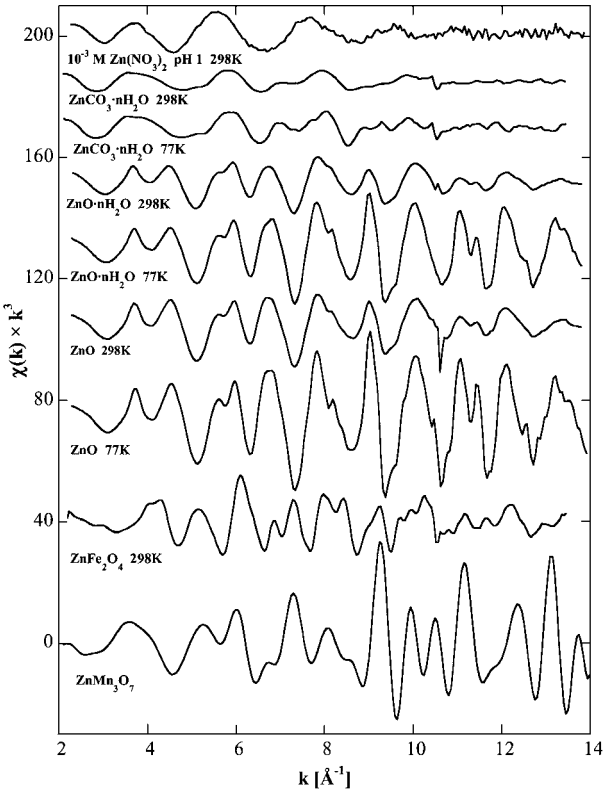

FIG. 1. Background-subtracted, normalized, and averaged k^3-weighted XAS spectra of Zn standards studied at Zn K-edge in transmission mode as a function of temperature. $ZnMn_3O_7$ structure is generated from crystallographic data using FEFF7 (34).

where the second-shell coordination numbers were fixed. The resulting first shell includes 5.2–5.6 O atoms at 2.12 Å, while the second shell showed good fits for four Zn atoms at 3.14 Å and two O atoms at 3.24 Å. No stable fits were obtained when carbon was included in the second shell; this may be due to the smaller single scattering contributions from carbon as compared to Zn and oxygen. Hesterberg *et al.* (42) reported the first shell for $ZnCO_3$ to consist of 6.2 O at 2.09 Å, while that of zinc hydroxy carbonate was comprised of 6.2 O atoms at 2.01 Å. For $Zn(NO_3)_{2(aq)}$, $ZnO \cdot nH_2O$ at 298 K, and $ZnCO_3 \cdot nH_2O$ at all temperatures, stable fits were obtained only when the third cumulant (C_3) was included, which is indicative of moderate disorder in their structures. In all other standards, the fits were well described by a Gaussian distribution. Temperature studies revealed a decrease in the Debye–Waller factor (σ^2) with a decrease in temperature as a result of a significant contribution by the thermal component of the Debye–Waller factor. This result demonstrates the moderate disorder in the structures of $ZnO \cdot nH_2O$ and $ZnCO_3 \cdot nH_2O$.

Zn–HFO Adsorption Samples

The XAS spectra for Zn–HFO adsorption systems studied as a function of pH, adsorbate loading, and scanning temperature appear to be similar to each other (Fig. 3) as well as to the

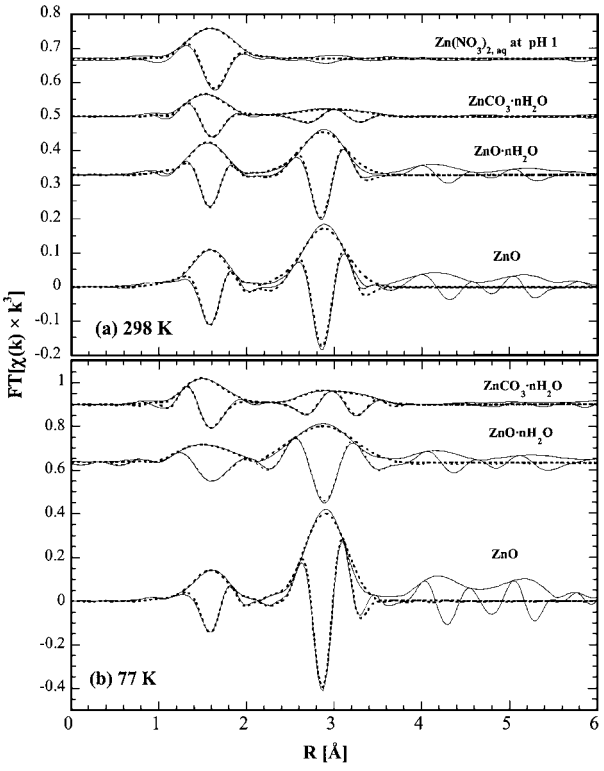

FIG. 2. Fourier transforms (solid lines) of Zn standards studied at (a) 298 K and (b) 77 K, filtered over 2.65–13.65 Å^{-1} (except $Zn(NO_3)_{2,aq}$ 2.3–9.2 Å^{-1}) and fitted (dashed lines) with $ZnMn_3O_7$ over 1.0–3.65 Å (except $ZnCO_3 \cdot nH_2O$ with hydrozincite over 0.6–3.8 Å and $Zn(NO_3)_{2,aq}$ with $ZnMn_3O_7$ over 0.5–2.20 Å).

spectrum of the aqueous Zn^{2+}. These spectra exhibit a glitch at 10.2 Å^{-1}, which is due to the presence of a fracture in the Si(111) crystal at the X-11A beamline. The data are noisier in the higher k range due to the highly disordered structure from HFO. Except for their magnitudes, these spectra resemble each other as a function of loading suggesting a similar adsorption reaction. Furthermore, adsorption does not appear to be a function of pH. Because these spectra are similar to aqueous Zn^{2+} spectra, it appears the only backscattering contribution is from the first shell of oxygen atoms.

Fourier transforms of these spectra filtered over the k-range 2.3–9.2 Å^{-1} show only one broad shell for all samples irrespective of adsorbate concentration, method of contact (Fig. 4), or pH (Fig. 5). Fitting this shell between 0.5 and 2.2 Å suggests the presence of 5.9–6.2 highly disordered oxygen atoms at an average radial distance of 2.18 Å. The absence of a second shell rules out the formation of any well-ordered Zn precipitates or a Zn–Fe solid solution. The results reveal that adsorption is best represented as an outer-sphere complex. Temperature dependence (Table 2 and Fig. 4) also confirms physical adsorption due to a significant contribution by the thermal component of the Debye–Waller factor. Additionally, because these structural parameters (Table 2) did not vary with the adsorbate loading or pH, an earlier hypothesis from macroscopic studies (10, 12, 13) that Zn sorbs to HFO through one average type of site is corroborated. The Zn–O distance in Zn–HFO samples is much shorter than those found for Sr, an alkaline earth metal, which was also found to be physically sorbed to HFO (26); the result

TABLE 1
XAS Spectra Data Analyses for Zn Standards[a]

Standards	Element	N (atoms)	R (Å)	σ^2 (Å^2)	C_3 (Å^3)	E_o shift (eV)
First Shell						
$Zn(NO_3)_{2,aq}$, 298 K	O	5.83 ± 0.39	2.18 ± 0.036	$3.9 \times 10^{-3} \pm 7.2 \times 10^{-4}$	$2.19 \times 10^{-4} \pm 3.0 \times 10^{-5}$	4.47 ± 1.10
ZnO, 77 K	O	3.58 ± 0.30 (*4*)	$1.96 \pm 1.0 \times 10^{-3}$ (*1.97*)	$2.06 \times 10^{-3} \pm 2.0 \times 10^{-4}$	—	1.23 ± 0.18
ZnO, 298 K	O	3.27 ± 0.01	$1.96 \pm 6.4 \times 10^{-4}$	$2.63 \times 10^{-3} \pm 5.9 \times 10^{-5}$	—	0.97 ± 0.06
$ZnO \cdot nH_2O$, 77 K	O	3.51 ± 0.22	$1.98 \pm 6.8 \times 10^{-3}$	$3.57 \times 10^{-3} \pm 2.6 \times 10^{-4}$	—	2.06 ± 0.31
$ZnO \cdot nH_2O$, 298 K	O	4.06 ± 0.01	$2.00 \pm 2.6 \times 10^{-3}$	$4.09 \times 10^{-3} \pm 8.5 \times 10^{-5}$	$4.30 \times 10^{-4} \pm 4.7 \times 10^{-5}$	1.88 ± 0.13
$ZnCO_3 \cdot nH_2O$, 77 K	O	5.6 ± 0.35 (*6*)	$2.11 \pm 6.7 \times 10^{-2}$ (*2.11*)	$4.44 \times 10^{-3} \pm 4.2 \times 10^{-4}$	$3.87 \times 10^{-4} \pm 1.1 \times 10^{-5}$	4.93 ± 0.10
$ZnCO_3 \cdot nH_2O$, 298 K	O	5.19 ± 0.66	$2.12 \pm 6.2 \times 10^{-2}$	$6.64 \times 10^{-3} \pm 3.0 \times 10^{-4}$	$1.04 \times 10^{-3} \pm 8.0 \times 10^{-5}$	3.76 ± 0.35
Second Shell						
Standards	Element	N (atoms)	R (Å)	σ^2 (Å^2)	C_3 (Å^3)	% Res.
$Zn(NO_3)_{2,aq}$, 298 K					—	2.37
ZnO, 77 K	Zn	12.75 ± 1.48 (*12*)	$3.22 \pm 8.5 \times 10^{-4}$ (*3.21*)	$4.45 \times 10^{-3} \pm 1.4 \times 10^{-4}$	—	7.16
ZnO, 298 K	Zn	11.69 ± 0.14	$3.21 \pm 5.6 \times 10^{-4}$	$9.47 \times 10^{-3} \pm 1.0 \times 10^{-4}$	—	10.25
$ZnO \cdot nH_2O$, 77 K	Zn	14.27 ± 0.17	$3.22 \pm 2.9 \times 10^{-3}$	$7.64 \times 10^{-3} \pm 2.8 \times 10^{-4}$	—	7.21
$ZnO \cdot nH_2O$, 298 K	Zn	10.54 ± 0.09	$3.24 \pm 1.9 \times 10^{-3}$	$1.10 \times 10^{-2} \pm 7.5 \times 10^{-5}$	$2.75 \times 10^{-4} \pm 1.2 \times 10^{-5}$	8.35
$ZnCO_3 \cdot nH_2O$, 77 K	Zn	4.00 (*4*)	$3.14 \pm 7.9 \times 10^{-2}$ (*3.18*)	$1.05 \times 10^{-2} \pm 2.0 \times 10^{-3}$	$-1.73 \times 10^{-4} \pm 6.7 \times 10^{-5}$	11.01
	O	2.00 (*2*)	3.24 (*3.24*)	$3.04 \times 10^{-2} \pm 7.8 \times 10^{-4}$	0.00	
$ZnCO_3 \cdot nH_2O$, 298 K	Zn	4.00	$3.09 \pm 5.2 \times 10^{-2}$	$1.79 \times 10^{-2} \pm 5.9 \times 10^{-4}$	$-2.17 \times 10^{-4} \pm 4.9 \times 10^{-5}$	12.08
	O	2.00	3.24	$4.02 \times 10^{-2} \pm 1.4 \times 10^{-3}$	0.00	

[a] Numbers in parentheses represent the corresponding structural parameters of the reference. Associated errors (standard deviations) presented with each averaged parameter result from individual scans. XAS spectra were Fourier transformed from 2.64 to 13.65 Å^{-1}, except for aqueous $Zn(NO_3)_2$ which was from 2.3 to 9.2 Å^{-1}. Two-shell fits ranged from 1.0 to 3.65 Å, except for aqueous $Zn(NO_3)_2$ which involved one shell from 0.5 to 2.2 Å.

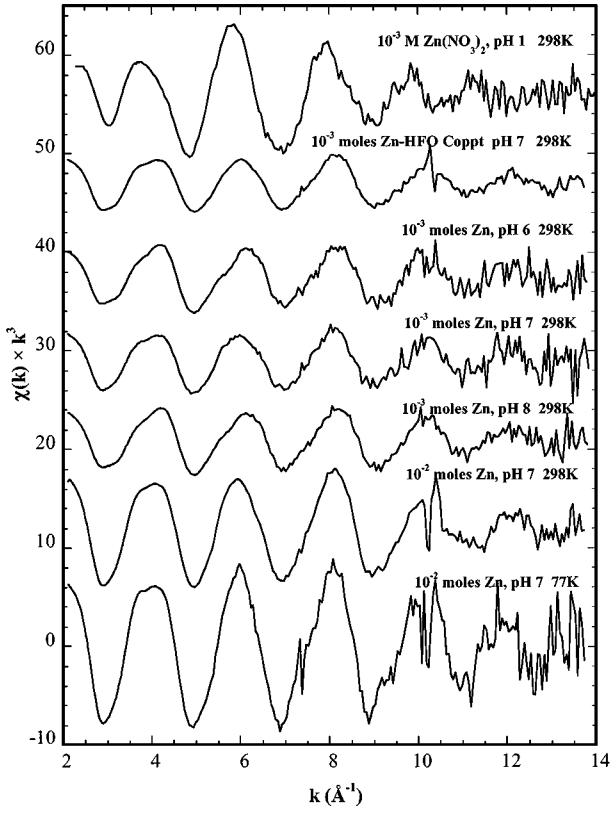

FIG. 3. Background-subtracted, normalized, and averaged k^3-weighted XAS spectra of Zn sorbed to 1 g L^{-1} HFO studied at Zn K-edge in fluorescence mode as a function of pH, adsorbate loading, and temperature compared with that of aqueous $Zn(NO_3)_2$ collected in transmission mode.

demonstrates the higher affinity of transition metals for HFO in comparison to that of alkaline earth metals (10, 12). The Zn–HFO coprecipitate was also found to exhibit a local structure consistent with the adsorption samples suggesting that Zn is only physically sorbed on the microporous surfaces (Fig. 4 and Table 2). Because Zn was present during the HFO precipitation, the ion could potentially sorb on the HFO nanoparticles prior to its aggregation and formation of microporous surfaces. Interestingly, through macroscopic studies, Crawford *et al.* (43) demonstrated that although the coprecipitation of metal ions like Zn and Ni with amorphous iron oxide is more efficient than adsorption, the free energy changes of these two processes are comparable.

Spadini *et al.* (6) found from their XAFS studies that Cd sorption complexes with two-line ferrihydrite are independent of pH and of adsorbate loading as well. They observed approximately one Fe atom at 3.32 Å and 3.50 Å from the central Cd atom (Table 3). Similarly, Scheinost *et al.* (17) could fit one Fe atom at 3.3 Å from either Cu or Pb sorbed to two types of two-line ferrihydrite (freshly precipitated and resuspended freeze-dried oxide). They further observed that this local structure of sorbed Cu or Pb ion was invariant of reaction time (up to 8 weeks), type of ferrihydrite, and presence of competing ions or fulvic acid.

Zn–Goethite Adsorption Samples

Zinc sorption to goethite was studied as a function of pH in the site saturation range as determined from macroscopic isotherm studies (11, 13). The averaged XAS spectra are similar in phase suggesting that the sorption mechanism does not change with pH (Fig. 6a). Interestingly, these spectra do not resemble those of aqueous $Zn(NO_3)_2$ or Zn–HFO systems suggesting that the local structure of Zn changes upon sorption to goethite. The presence of a second back scatterer is indicative of a second shell. Thermodynamic analyses from macroscopic experiments indicate that Zn adsorption to goethite is an endothermic chemical type of reaction resulting in the formation of inner-sphere complexes (13, 14).

To further test the type of adsorption mechanism, spectra were fit with a theoretical standard generated by substituting Mn ions in chalcophanite with Fe ions as described in the XAS analyses section. Accordingly, results (Fig. 6b and Table 2) show that the first shell is disordered and consists of approximately four oxygen atoms at an average radial distance of 1.97 Å. These parameters suggest that Zn ions do not retain their octahedral hydration shell upon adsorption to goethite. Waychunas *et al.* (29) also found that upon sorption to ferrihydrite, Zn^{2+} ions were converted from octahedral configuration to a tetrahedral

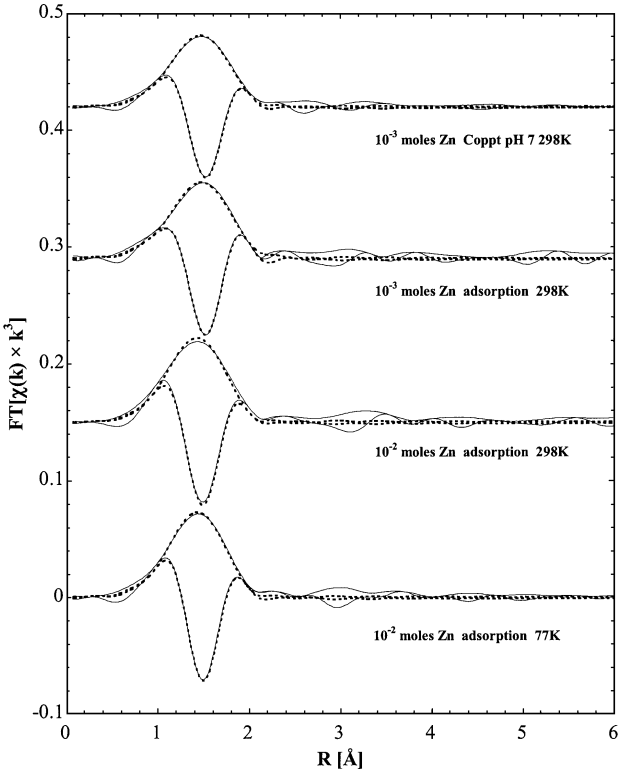

FIG. 4. Fourier transforms (solid lines) of Zn K-edge XAS spectra of Zn sorbed to 1 g L^{-1} HFO at pH 7, presented as a function of Zn concentration, method of contact, and temperature, each filtered over the k range 2.3–9.2 $Å^{-1}$ and fitted with chalcophanite (dashed lines) from 0.5 to 2.20 Å.

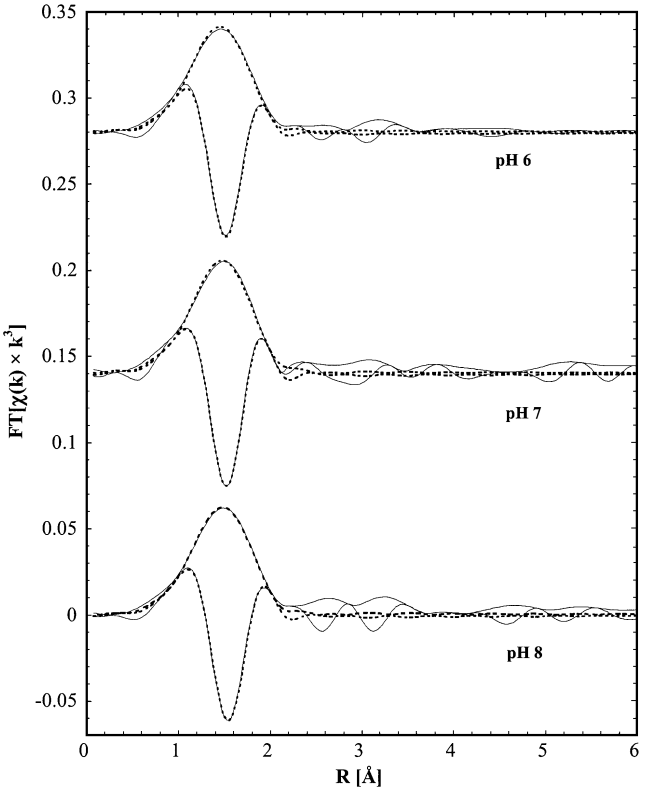

FIG. 5. Fourier transforms (solid lines) of Zn K-edge XAS spectra of 10^{-3} mol of Zn sorbed to HFO (1 g L^{-1}) at 25°C, presented as a function of pH, each filtered over the *k* range 2.3–9.2 $Å^{-1}$ and fitted with chalcophanite (dashed lines) from 0.5 to 2.20 Å.

one. As discussed earlier, Trainor *et al.* (30) observed that at low sorption densities (<1.1 μmol m^{-2}) Zn^{2+} sorbs to alumina as a mononuclear innersphere complex with tetragonal first-shell coordination and an average Zn–O distance of 1.96 Å. Trainor *et al.* (30) also observed two additional oxygen atoms in the first shell at the higher sorption densities; however, they argue that given the short Zn–O distances (2.01–2.04 Å) in the first shell, these additional oxygens may be from the alumina surface resulting in a distorted octahedra. In contrast, Zn sorbed to HFO (in this study), to goethite (21), and to pyrophyllite (31) appeared to retain its six-fold oxygen coordination. One potential reason for differing results between Schlegel *et al.* (21) and this goethite work is the degree of oxide crystallinity.

In the Zn–goethite systems, the second shell was best fitted with 1.7–2.4 Fe atoms at 2.49–2.51 Å (Table 2) suggesting that Zn ions are chemically sorbed to goethite forming an innersphere complex. These results are in agreement with the high adsorption enthalpies noted for Zn and Ni sorption to goethite (13). No fits were obtained with oxygen or Zn in the second shell. The structural parameters for Zn–goethite systems show very little temperature dependence (Table 2) suggesting greater static contributions as compared to thermal ones. This temperature effect is consistent with chemical bonding. The Zn–Fe distances observed in this research are comparable to the many other systems studied (Table 3); for example Cd–Fe distances found for Cd adsorption to goethite are 3.26 and 3.48 Å, where the Fe coordination number at 3.48 Å is 3 times greater than that at 3.26 Å (6). Using γ-FeOOH to fit the second shell for Zn sorbed to goethite, Schlegel *et al.* (21) estimated 0.9 Fe atoms at

TABLE 2
XAS Parameters of Zn–HFO and Zn–Goethite Adsorption Samples Filtered from 2.3 to 9.2 $Å^{-1}$[a]

Zn loadings (mol g^{-1})	Adsorbent	*T* (K)	*N* (atoms)	*R* (Å)	σ^2 ($Å^2$)	C_3 ($Å^3$)	E_o shift (eV)	% Res
First Shell: Oxygen								
10^{-2}, pH 7	HFO	77	6.19 ± 0.28	$2.18 \pm 2.3 \times 10^{-3}$	$8.83 \times 10^{-3} \pm 6.6 \times 10^{-4}$	$-1.00 \times 10^{-4} \pm 3.4 \times 10^{-4}$	2.56 ± 0.86	4.09
10^{-2}, pH 7	HFO	298	5.92 ± 0.24	$2.19 \pm 4.8 \times 10^{-3}$	$9.11 \times 10^{-3} \pm 6.5 \times 10^{-4}$	$-9.40 \times 10^{-4} \pm 4.0 \times 10^{-4}$	5.37 ± 1.69	5.21
10^{-3}, pH 8	HFO	298	6.08 ± 0.26	$2.18 \pm 3.2 \times 10^{-3}$	$8.10 \times 10^{-3} \pm 9.3 \times 10^{-4}$	$-8.70 \times 10^{-4} \pm 2.9 \times 10^{-4}$	3.56 ± 0.31	5.51
10^{-3}, pH 7	HFO	298	6.103 ± 0.53	$2.18 \pm 3.7 \times 10^{-3}$	$9.99 \times 10^{-3} \pm 2.06 \times 10^{-3}$	$-9.98 \times 10^{-4} \pm 3.3 \times 10^{-4}$	3.32 ± 0.98	4.63
10^{-3}, pH 6	HFO	298	6.11 ± 0.51	$2.18 \pm 2.3 \times 10^{-3}$	$9.66 \times 10^{-3} \pm 4.1 \times 10^{-4}$	$-1.52 \times 10^{-4} \pm 1.9 \times 10^{-4}$	3.55 ± 0.97	7.52
10^{-3}, pH 7[b]	HFO	298	6.21 ± 0.35	$2.18 \pm 4.2 \times 10^{-3}$	$9.55 \times 10^{-3} \pm 7.6 \times 10^{-4}$	$-4.99 \times 10^{-4} \pm 2.2 \times 10^{-4}$	3.50 ± 1.09	5.16
1.2×10^{-5}, pH 6	Goethite	77	3.95 ± 0.53	$1.97 \pm 2.8 \times 10^{-3}$	$9.39 \times 10^{-3} \pm 8.5 \times 10^{-4}$	$-5.65 \times 10^{-4} \pm 1.1 \times 10^{-4}$	9.37 ± 0.70	8.78
2.0×10^{-5}, pH 7	Goethite	77	3.94 ± 0.43	$1.97 \pm 2.1 \times 10^{-3}$	$9.91 \times 10^{-3} \pm 3.6 \times 10^{-4}$	$-2.54 \times 10^{-4} \pm 3.8 \times 10^{-5}$	9.10 ± 0.58	8.19
1.2×10^{-5}, pH 6	Goethite	298	4.04 ± 0.36	$1.97 \pm 4.0 \times 10^{-3}$	$9.50 \times 10^{-3} \pm 1.3 \times 10^{-3}$	$-3.26 \times 10^{-4} \pm 4.5 \times 10^{-4}$	1.90 ± 0.90	9.86
2.0×10^{-5}, pH 7	Goethite	298	4.09 ± 0.37	$1.97 \pm 5.1 \times 10^{-3}$	$1.06 \times 10^{-2} \pm 9.9 \times 10^{-4}$	$-6.60 \times 10^{-5} \pm 3.8 \times 10^{-5}$	2.16 ± 0.69	6.72
Second Shell: Iron								
1.2×10^{-5}, pH 6	Goethite	77	2.84 ± 0.55	$3.54 \pm 3.1 \times 10^{-3}$	$1.35 \times 10^{-2} \pm 1.5 \times 10^{-4}$	$-3.35 \times 10^{-4} \pm 2.1 \times 10^{-4}$	9.37 ± 0.70	8.78
2.0×10^{-5}, pH 7	Goethite	77	2.89 ± 0.14	$3.54 \pm 2.4 \times 10^{-3}$	$1.01 \times 10^{-2} \pm 3.1 \times 10^{-4}$	$-3.89 \times 10^{-5} \pm 2.6 \times 10^{-5}$	9.10 ± 0.58	8.19
1.2×10^{-5}, pH 6	Goethite	298	1.74 ± 0.32	$3.52 \pm 4.8 \times 10^{-3}$	$1.43 \times 10^{-2} \pm 2.6 \times 10^{-3}$	$-4.81 \times 10^{-4} \pm 3.9 \times 10^{-4}$	1.90 ± 0.90	9.86
2.0×10^{-5}, pH 7	Goethite	298	2.49 ± 0.29	$3.51 \pm 1.9 \times 10^{-2}$	$1.08 \times 10^{-2} \pm 2.5 \times 10^{-3}$	$-5.94 \times 10^{-5} \pm 3.6 \times 10^{-5}$	2.16 ± 0.69	6.72

[a] Errors provided with the parameters are based on standard deviations resulting from individual scans. Typically the uncertainties in N are estimated to be 20% for the first shell and 30% for the second shell. Similarly, variations in *R* are estimated to be 0.03 Å for all shells. For goethite adsorption samples multiple shells were fitted over 0.5–4.2 Å and for all HFO samples were fitted over 0.5–2.2 Å.

[b] Sample prepared by coprecipitating 10^{-3} mol of Zn with HFO (1 g L^{-1}) at pH 7 and aging for 4 h.

TABLE 3
Other Relevant XAS Studies at Room Temperature

References	Oxide[a]	Adsorbate	pH	First Shell (Oxygen)		Additional Shells		
				N	*R* (Å)	Element	*N*	*R* (Å)
18[b]	G	Cr^{3+}	4.0	[c]	[c]	Fe, Cr	1.1	3.01
						Fe, Cr	0.8	3.45
						Fe, Cr	1.2–1.9	3.95–3.99
	F	Cr^{3+}	4.0	[c]	[c]	Fe, Cr	2.1–3.0	3.00–3.05
						Fe, Cr	0.4–0.8	3.40–3.46
						Fe, Cr	1.5–2.2	3.95–4.03
5	G	SeO_4^{2-}	3.5	4.0	1.65	Fe	2.0	3.29
	F	SeO_4^{2-}	3.5	4.0	1.65	Se or Fe	0.4	2.76 or 2.80
						Fe	1.8	3.30
6	G	Cd^{2+}	7.5	5.5–6.2	2.30	Fe	0.2–0.7	3.24–3.31
						Fe	0.6–1.2	3.46–3.51
	F	Cd^{2+}	6.7–9.5	4.0–5.0	2.27–2.31	Fe	0.7	3.32
						Fe	0.8	3.50
22	G	Pb^{2+}	6.0–7.0	2.2–2.4	2.26–2.27	Fe	0.2–0.3	3.31–3.36
	H	Pb^{2+}	6.0–8.0	2.0–2.4	2.27–2.30	Fe	0.2–0.5	3.27–3.31
20	G	AsO_4^{3-}	6.0–9.0	3.7–3.9	1.66–1.67	Fe	0.6–1.3	2.84–2.85
						Fe	1.0–1.6	3.23–3.24
						Fe	0.4–1.1	3.59–3.60
	G	CrO_4^{2-}	5.0–6.0	3.9	1.68–1.69	Fe	0.4–1.0	2.91–3.29
							0.8–1.5	3.27–3.63
21	G	Zn^{2+}	7.0	6.0	2.10	Fe	0.9	3.00
							1.2	3.20
23	G	Pb^{2+}	5.0–7.0	2.1–2.9	2.26–2.33	Fe	0.3–0.7	3.00–3.36
							0.3–1.1	3.86–3.93
42	G	AsO_4^{3-}	6.4–8.6	3.0–3.1	1.78–1.79	Fe	2.3–2.4	3.36–3.40
24	G	$Pb^{2+}/H_2PO_4^-$	5.5	4.0	2.30	Fe	1.6	3.35
25	G	Hg^{2+}	4.6	2.0	2.04	Fe	1.0	3.28
28	G	Sr^{2+}	6.4–8.6	8.2–9.7	2.58–2.61	[d]	[d]	[d]
			8.46–9.9	8.3–10.1	2.58–2.63	C	0.4–3.8	3.03–3.05
						Sr	1.5–3.3	4.13–4.90

[a] G, goethite; F, two-line ferrihydrite; H, hematite.
[b] Fe and Cr equally contribute to the second shell and the corresponding *R* represents the averaged distance over both metals.
[c] Shells not reported.
[d] No shells observed.

3.00 Å and 1.2 Fe atoms at 3.20 Å. On the other hand, ZnEDTA, upon sorption to goethite, maintained its local structure similar to that in the aqueous phase (21). As discussed above, Scheinost *et al.* (17) conducted kinetic studies for Cu and Pb sorption to two-line ferrihydrite in single and binary systems, where one Fe atom was observed in the second shell for either Cu or Pb. Mercury was also found to form an inner-sphere adsorption complex with goethite at pH 4.6, where its first shell contained approximately two oxygen atoms at 2.04 Å and the second shell consisted of approximately one Fe atom at 3.28 Å and 3.82 Å (25). From XAS studies of Pb sorption to goethite and hematite, Bargar *et al.* (22, 23) proposed that Pb ions formed mononuclear sorption complexes with Fe ions in the second shell at 3.27–3.31 Å for hematite and at 3.31–3.36 Å for goethite. However, no Pb atoms were observed in the second shell for Pb and Pb–chloro adsorption complexes indicative of the absence of Pb precipitates. In chromate sorption to goethite, second-shell contributions included two Fe atoms with one at 2.91 Å and the other at 3.29 Å, while in an As(V)–goethite system, Fe atoms were observed at 2.85 Å, 3.24 Å, and 3.59 Å (20). For arsenite, a bidentate complex was found with Fe atoms located at 3.378 Å (44). On the other hand, O'Day *et al.* (1) studied a zinc–iron oxyhydroxide coprecipitate, where they fitted the first shell with two oxygens at 1.92 and 2.04 Å and the second shell with a mixture of 1.2 Zn atoms at 3.54 Å and 0.7 Fe atoms at 3.12 Å. Trainor *et al.* (30) also observed a mixed Zn/Al second shell at 3.05 Å where the coordination number increased with sorption density (30). In another interesting study, Manceau *et al.* (45) prepared Zn–goethite by aging Zn–ferrihydrite coprecipitate under alkaline conditions at 70°C for 93 days. The resultant oxide was found to have a first shell comprising two O subshells: $N_1 = 1.1$ at 1.87 Å and $N_2 = 5.4$ at 2.05 Å, while the second shell exhibited a wide distribution of Fe atoms with radial distances ranging from 3.0 to 3.48 Å.

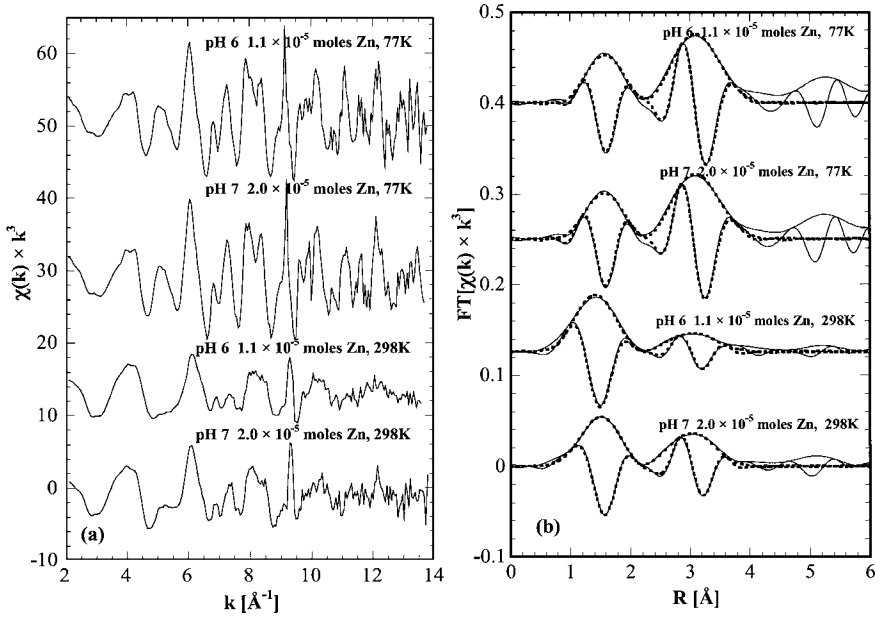

FIG. 6. (a) Background-subtracted, normalized, and averaged k^3-weighted XAS spectra of Zn sorbed to goethite (1 g L^{-1}) studied in fluorescence mode using a Ge solid-state detector presented with (b) corresponding Fourier transforms (solid lines) fitted with (dashed lines) Fe-substituted chalcophanite standard generated with FEFF7. The *k* range for Fourier transforms is 2.3–9.2 $Å^{-1}$ while the *R* window for multishell fitting is 0.5–4.20 Å.

SUMMARY

Based on the spectroscopic evidence presented, the Zn ion physically sorbs to amorphous oxides such as HFO where it retains its hydration shell upon adsorption. The absence of Zn contributions in the second shell rules out the possibility of polynuclear complexes or any well-ordered Zn precipitates. Furthermore, the lack of contributions from Fe in the second shell suggests an outer-sphere type of adsorption mechanism that is independent of pH and adsorbate concentration. Similarly, the local structure from the coprecipitate sample suggests that Zn is only physically sorbed on the microporous surfaces of HFO and does not appear to form any solid solution with ferric ions. On the other hand, Zn ions form strongly bonded mononuclear complexes with goethite where their octahedral hydration shell is converted into a tetragonal structure upon adsorption. Overall, the results presented in this paper demonstrate that even though the local structures of HFO and goethite are found to have similarities, they do not exhibit similar sorption properties. HFO is viewed as a mosaic of short octahedral chains resulting in a greater sorption capacity than goethite. Most importantly, this research aids in selecting mechanistic models for describing the fate of metals like Zn in soils and sediments that are rich in iron oxides.

ACKNOWLEDGMENTS

This research was supported by NSF Grants BES-9753072 and BES-0089903, start-up funds granted to L.A. from the New Jersey Institute of Technology, and the DuPont Young Professors and Aid to Education Grants. The authors thank James Dyer at DuPont Engineering Technology for his input and support.

REFERENCES

1. O'Day, P. A., Carroll, S. A., and Waychunas, G. A., *Environ. Sci. Technol.* **32,** 943 (1998).
2. Martinez, C. E., and McBride, M. B., *Environ. Sci. Technol.* **33,** 745 (1999).
3. Schwertmann, U., and Taylor, R. M., *in* "Minerals in Soil Environments" (J. B. Dixon and S. B. Weed, Eds.), 2nd Ed., SSSA Book Series No. 1, p. 379, Soil Science Soc. of America, Madison, WI, 1989.
4. Manceau, A., and Combes, J. M., *Phys. Chem. Miner.* **15,** 283 (1988).
5. Manceau, A., and Charlet, L., *J. Colloid Interface Sci.* **168,** 87 (1994).
6. Spadini, L., Manceau, A., Schindler, P. W., and Charlet, L., *J. Colloid Interface Sci.* **168,** 73 (1994).
7. Okazaki, M., Takamidoh, K., and Yamane, I., *Soil Sci. Plant Nutr.* **32,** 523 (1986).
8. Axe, L., and Anderson, P., *J. Colloid Interface Sci.* **175,** 157 (1995).
9. Axe, L., and Anderson, P., *J. Colloid Interface Sci.* **185,** 436 (1997).
10. Trivedi, P., and Axe, L., *Environ. Sci. Technol.* **34,** 2215 (2000).
11. Trivedi, P., Axe, L., and Dyer, J., *Colloids Surf.* **191,** 107–121 (2001).
12. Trivedi, P., and Axe, L., *Environ. Sci. Technol.* **35,** 1779 (2001).
13. Trivedi, P., and Axe, L., *J. Colloid Interface Sci.* **244,** 221–229 (2001).
14. Rodda, D. P., Johnson, B. B., and Wells, J. D., *J. Colloid Interface Sci.* **168,** 87 (1996).
15. Misak, N. Z., Ghoneimy, H. F., and Morcos, T. N., *J. Colloid Interface Sci.* **184,** 31 (1996).
16. Barrow, N. J., Gerth, J., and Brümmer, G. W., *J. Soil Sci.* **40,** 437 (1989).
17. Scheinost, A. C., Abend, S., Pandya, K. I., and Sparks, D. L., *Environ. Sci. Technol.* **35,** 1090 (2001).
18. Charlet, L., and Manceau, A. A., *J. Colloid Interface Sci.* **148,** 443 (1992).
19. Waite, T. D., Davis, J. A., Payne, T. E., Waychunas, G. A., and Xu, N., *Geochim. Cosmochim. Acta* **58,** 5465 (1994).
20. Fendorf, S., Eick, M. J., Grossl, P., and Sparks, D. L., *Environ. Sci. Technol.* **31,** 315 (1997).
21. Schlegel, M. L., Manceau, A., and Charlet, L., *J. Phys. IV Fr.* **7C-3,** 823 (1997).
22. Bargar, J. R., Brown, Jr., G. E., and Parks, G. A., *Geochim. Cosmochim. Acta* **61,** 2639 (1997).

23. Bargar, J. R., Brown, Jr., G. E., and Parks, G. A., *Geochim. Cosmochim. Acta* **62,** 193 (1998).
24. Weesner, F. J., and Bleam, W. F., *J. Colloid Interface Sci.* **205,** 380 (1998).
25. Collins, C. R., Sherman, D. M., and Ragnarsdottir, K. V., *J. Colloid Interface Sci.* **219,** 345 (1999).
26. Axe, L., Bunker, G. B., Anderson, P. R., and Tyson, T. A., *J. Colloid Interface Sci.* **199,** 44 (1998).
27. Bargar, J. R., Persson, P., and Brown, Jr., G. E., *Geochim. Cosmochim. Acta* **63,** 2957 (1999).
28. Sahai, N., Carroll, S. A., Roberts, S., and O'Day, P. A., *J. Colloid Interface Sci.* **222,** 198 (2000).
29. Waychunas, G. A., Fuller, C. C., and Davis, J. A., *in* "1994 Activity Report," Stanford Synchrotron Radiation Laboratory Report, p. 78. DOE, Stanford, CA, 1995.
30. Trainor, T. P., Brown, Jr., G. E., and Parks, G. A., *J. Colloid Interface Sci.* **231,** 359 (2000).
31. Ford, R. G., and Sparks, D. L., *Environ. Sci. Technol.* **34,** 2479 (2000).
32. Dzombak, D. A., and Morel, F. M. M., *J. Colloid Interface Sci.* **112,** 588 (1986).
33. Trivedi, P., and Axe, L., *J. Colloid Interface Sci.* **218,** 554 (1999).
34. Ressler, T., *J. Phys. IV* **7,** 269 (1997).
35. Zabinsky, S. I., Reher, J. J., Ankudinov, A., Albers, R. C., and Eller, M. J., *Phys. Rev. B* **52,** 2995 (1995).
36. Post, J. E., and Appleman, D. E., *Am. Mineral.* **73,** 1401 (1988).
37. Wyckoff, R. W. G., "Crystal Structures: Volume 1," 2nd Ed. Wiley, New York, 1963.
38. Post, J. E., *Proc. Natl. Acad. Sci. U.S.A.* **96,** 3447 (1999).
39. Ghose, S., *Acta Crystallogr.* **17,** 1051 (1963).
40. Numako, C., and Nakai, I., *Spectrochim. Acta: Part B* **54,** 133 (1999).
41. Pandya, K. I., Russell, A. E., McBreen, J., and O'Grady, W. E., *J. Phys. Chem.* **99,** 11967 (1995).
42. Hesterberg, D., Sayers, D. E., Zhou, W., Plummer, G. M., and Robarge, W. P., *Environ. Sci. Technol.* **31,** 2840 (1997).
43. Crawford, R. J., Harding, I. H., and Mainwaring, D. E., *Langmuir* **9,** 3050 (1993).
44. Manning, B. A., Fendorf, S. E., and Goldberg, S., *Environ. Sci. Technol.* **32,** 2383 (1998).
45. Manceau, A., Schlegel, M. L., Musso, M., Sole, V. A., Gauthier, C., Petit, P. E., and Trolard, F., *Geochim. Cosmochim. Acta* **64,** 3643 (2000).